Highly Mixed Phases in Ball-milled Cu/ZnO Catalysts: An EXAFS and XANES Study

Didier Grandjean,[†] Hessel L. Castricum,[‡] Johannes C. van den Heuvel,*[,‡] and Bert M. Weckhuysen*[,†]

Inorganic Chemistry and Catalysis, Department of Chemistry, Utrecht University, Sorbonnelaan 16, 3584 CA Utrecht, The Netherlands, and Van't Hoff Institute for Molecular Sciences, University of Amsterdam, Nieuwe Achtergracht 166, 1018 WV Amsterdam, The Netherlands

Received: October 12, 2005; In Final Form: July 7, 2006

New highly mixed phases have been identified in Cu/ZnO systems by EXAFS and XANES at both the Cu and Zn K-edge. The phases were generated by ball-milling Cu_2O/ZnO mixtures under three different atmospheres of synthetic air (SA), SA + CO_2 and CO_2. The system milled in CO_2 shows disproportionation of Cu_2O into Cu^0, Cu^{1+} (cuprite Cu_2O-type phase) and Cu^{2+} (tenorite CuO-type phase), while most of the Zn^{2+} is transformed into a nanocrystalline/amorphous ZnO-type zincite that forms a superficial mixture of oxide and carbonate phases. When synthetic air is added to the CO_2 atmosphere, ball milling results in the oxidation of nearly half the Cu^{1+} into Cu^{2+} with no Cu metal formed. The copper phase in this material is almost entirely amorphous. In SA, a significant amount of Cu^{2+}- and Zn^{2+}-based phases appears to react to form a nanocrystalline/amorphous $Cu_{1-x}Zn_xO$ ($x \approx 0.3$) solid solution. This distorted rock saltlike solid solution, in which Zn and Cu feature different octahedral environments, was never reported before. It is thought to be formed by incorporation of Zn^{2+} in the Cu fcc sublattice of the cuprite Cu_2O matrix and the concomitant oxidation of Cu^{1+} into Cu^{2+}. The formation of such a highly mixed $Cu_{1-x}Zn_xO$ phase indicates strong Cu/Zn interaction in the Cu/ZnO system, which also suggests the presence of highly mixed phases in conventionally prepared activated catalysts.

1. Introduction

Copper-containing catalysts are widely used in industry for (de)hydrogenation of organic functional groups.[1,2] Among them, the Cu/ZnO system has been studied extensively, but despite decades of research, controversy still exists about the nature of the active site.[3−8] In the literature, a consensus has been reached that a high activity is obtained when an intimate mixture of Cu and ZnO (or Cu−Zn−Al/Cr) is achieved.[9,10] This is the reason that Cu/ZnO catalysts are conventionally prepared by coprecipitation of $Cu(NO_3)_2$ and $Zn(NO_3)_2$ solutions with subsequent aging and calcination. A vast amount of work has been carried out to find preparation methods that favor the formation of specific mixed phases, as a relationship was found between such structures and the activity of the reduced catalyst.

An alternative way to prepare highly mixed catalyst systems is to use a mechanochemical method,[11−14] introduced by Castricum et al.[15,16] as a promising route to obtain Cu/ZnO catalysts. An important feature of this technique is that, during milling, the surfaces of individual particles interact strongly with each other and with the gas atmosphere. Milling is considered to cause brief periods of very localized activation, which can be interpreted as strong local heating, followed by rapid quenching.[17,18] This can lead to the formation of metastable phases, that is, structures for which kinetics are too slow to restore thermodynamic equilibrium within a reasonable period of time. Prolonged milling leads to the formation of these surface phases in bulk quantities. Consequently, ball milling of CuO_x/ZnO mixtures is likely to produce intimately mixed precursors for the highly active methanol synthesis catalyst.

As a relationship between catalytic activity and mild surface oxidation of metallic Cu to Cu_2O was found,[8] we have investigated three new Cu/ZnO materials prepared by ball milling Cu_2O and ZnO under gas atmospheres of different oxidative power. Although these ball-milled materials differ from conventionally prepared Cu/Zn catalysts, previous catalytic tests have demonstrated their methanol synthesis activity after activation in H_2 and exposure to a CO/H_2 reaction mixture.[16] A variety of physical techniques have been used to characterize these new materials, such as high-resolution transmission electron microscopy (TEM), X-ray diffraction, and N_2 physisorption. Chemical characterization has been carried out by means of temperature-programmed reduction (TPR), N_2O chemisorption to determine the specific Cu^0 surface area, and low-pressure methanol synthesis activity. However, these techniques have all shown limitations regarding the complex nature of these multiphased systems, related to their nanocrystalline and amorphous nature. Indeed, as XRD is sensitive only to structures with long-range order, interpretation of patterns may be ambiguous. Electron microscopy can achieve direct imaging of the particles, but amorphous parts may be difficult to interpret and local sample areas may not be representative. Crucial information like the bulk Cu and Zn oxidation states and the short-range order of the amorphous domains is difficult to obtain using only these techniques.

X-ray absorption spectroscopy (XAS) is particularly well suited to characterize structures and bond distances in materials that lack detectable long-range order such as Cu-based catalysts[19] and also gives insight into their electronic structure. XAS is element specific and allows us to investigate the local order

* To whom correspondence should be addressed. E-mail: b.m.weckhuysen@chem.uu.nl; heuvel@science.uva.nl. Tel: +31 20 525 5265. Fax: + 31 20 525 5604.
[†] Utrecht University.
[‡] University of Amsterdam.

10.1021/jp055820i CCC: $33.50
Published on Web 08/09/2006

around Cu and Zn independently. For these reasons, XAS has been applied extensively to characterize several Cu/ZnO systems,[20−26] and important information such as oxidation states and nanocrystallite sizes could be obtained. Although a variety of Cu/Zn catalysts were investigated at the Cu K-edge, only few studies at the Zn K-edge[24,26] have been reported, likely due to the bulk nature of the Zn phase when ZnO is used as a support material.

We present here an EXAFS and XANES study at both the Cu and Zn K-edge in three systems obtained after ball milling Cu_2O/ZnO in different atmospheres. The aim of this study is to determine the short-range order in these materials and to identify all the phases. This XAS investigation is crucial to achieve a better understanding of the complex Cu/Zn interaction in these systems during preparation and in the active state.

2. Experimental Section

2.1. Preparation of the Ball-milled Materials. Three different materials have been prepared by ball milling cuprite Cu_2O and zincite ZnO mixtures (Cu/Zn atomic ratio 30:70) in synthetic air (BM_{SA}), synthetic air plus CO_2 (BM_{SA+CO_2}), and pure CO_2 (BM_{CO_2}). Typically 2 g of material was milled during 200 h in a vibratory mill.[18] Cu_2O (99%, <74 μm) and ZnO (99.995%, <74 μm) powders were purchased from CERAC (Milwaukee, USA). Milling in SA (20% O_2 in N_2, 99.999%) and CO_2 (99.998%) took place under a total pressure of 2 bar, after 2 cycles of evacuation to 10^{-6} mbar and filling the vial with gas. Leakage could be neglected, since the mill was specially designed for high-vacuum applications. For the milling in SA plus CO_2, partial O_2 and CO_2 pressures were set approximately equal at 0.4 bar (total pressure of 2.4 bar). Ambient air was not considered because of climatic variations. XRD patterns taken over a period of several years showed that these materials exhibited excellent structural stability.

2.2. Electron Microscopy and X-ray Diffraction. High-resolution TEM and electron diffraction were performed on a Philips CM30UT electron microscope operated at 300 kV. XRD patterns were recorded with an Enraf Nonius CPS-120 diffractometer using Cu Kα radiation. Crystallite sizes were calculated from the widths of the diffraction lines with the Scherrer formula after correction for instrumental broadening.

2.3. X-ray Absorption Spectroscopy. X-ray absorption data were collected on DUBBLE beamline (BM26A) at the European Synchrotron Radiation Facility (Grenoble, France), typically operating at 6 GeV, 200 mA, and $2 \times 1/3$ filling mode using a Si(111) double-crystal monochromator. Appropriate amounts of sample were finely ground with BN and pressed (2 bar) into ø 13×0.5 mm^3 pellets producing a suitable edge jump. XAS signals were measured in transmission mode both at the Cu K-edge (8978.9 eV) and the Zn K-edge (9658.6 eV). Cu_2O, CuO (99.9%, <74 μm), and ZnO powders from CERAC and standard Cu foil were used as references. Ionization chambers were filled with standard Ar/He mixtures. Cu and Zn K-edges were collected in the same dataset with acquisition times up to 80 min (1−6 s/point).

Data reduction of the spectra was performed with the program EXBROOK.[27] Preedge background subtraction and normalization was carried out by fitting a linear polynomial to the preedge region and cubic splines to the postedge region of the absorption spectrum. EXAFS refinements were performed with the EXCURV98 package.[27] Phase shifts and backscattering factors were calculated ab initio using Hedin−Lundqvist potentials. Refinements were carried out using k^3 weighting in the range 3.5−12 Å^{-1}. Anharmonicity effects of Cu^0 were corrected by the cumulant expansion feature in EXCURV98 using a linear expansion coefficient of 17.1×10^{-6} K^{-1}. The AFAC factors (amplitude reduction due to many-electron processes) calibrated from the EXAFS fits of the metal foils were fixed at 0.9 and 1.0 at the Cu and Zn K-edge, respectively. Due to the highly amorphous character of the Cu phases, the oscillations of the Cu K-edge EXAFS continuing beyond the Zn K-edge are significantly damped at $k > 13-14$ Å^{-1} and did not affect the EXAFS analysis at the Zn edge.

3. Results and Discussion

3.1. XRD and HRTEM. Figure 1 presents the HRTEM images of the ball-milled materials BM_{SA}, BM_{SA+CO_2}, and BM_{CO_2}, whereas Figure 2 shows their corresponding XRD patterns. The TEM measurements showed that all materials had a nanocrystalline character and a relatively similar morphology. The XRD patterns of BM_{CO_2} and BM_{SA+CO_2} show broad reflections belonging to the ZnO phase. Except for the CuO shoulder at $2\theta = 38.47$ °, no clear Cu_2O or CuO peaks can be detected, which indicates that Cu is present in either amorphous or nanocrystalline phases. Interestingly, XRD showed a significant amount of Cu^0 is present in BM_{CO_2}, indicating that some reduction of Cu_2O has occurred due to the low O_2 partial pressure. Part of the Cu_2O phase was apparently transformed into Cu^0, visible in the XRD pattern, and possibly into an amorphous CuO phase. Reduction also becomes clear from the decrease in the TPR Cu oxidation level, amounting to 50% for Cu^{1+} but decreasing significantly to 34% in the ball-milled material. Previous XRD results obtained after ball milling the bulk reference compounds CuO and ZnO in a CO_2 atmosphere indicated the formation of amorphous carbonates.[16] In the current materials, carbonate formation was also evidenced by TGA-MS, as decomposition into CO_2, and oxides took place during heating in argon. Significant amounts of carbonate were found to be present (Table 1), amounting to $^1/_3$ of the total number of anions present, with the remainder consisting of O^{2-} anions. Average crystallite sizes determined by XRD were 5 nm Cu metal, 8 nm ZnO for BM_{CO_2}, and 11 nm ZnO for BM_{SA+CO_2}. These results were confirmed by TEM measurements that showed crystallites of sizes ranging from 3 to 20 nm; electron diffraction showed the same lines as XRD.

The XRD pattern of BM_{SA} shows the typical broadening resulting from the milling process.[16] However, the ZnO reflections feature a stronger broadening and significantly lower intensity than in the two other materials. This indicates that the ZnO phase is more amorphous in BM_{SA} and that additionally part of ZnO may have been transformed into another phase. Two intense and broad diffraction peaks, apparently corresponding to a nanocrystalline Cu_2O phase, are also present. HRTEM measurements on BM_{SA} (Figure 1a) show that this material is relatively well crystallized with sizes ranging between 2 and 8 nm. However, the presence of a significant amount of Cu^{1+} in a material ball milled in synthetic air would be remarkable, especially when it is considered that previous TPR measurements (Table 1) pointed toward nearly complete mechanochemical oxidation of copper into Cu^{2+}. Moreover, a previous XRD study showed that a pure Cu_2O phase was entirely transformed into a CuO phase after ball milling in synthetic air.[16] The contradiction with the XRD interpretation suggests that these two reflections do not belong to the Cu_2O phase but to another phase resulting from a strong Cu/Zn interaction. Obviously, XRD/HRTEM results for BM_{SA} do not provide a full and convincing picture of the actual chemical and physical structure of this material. More generally, the extent

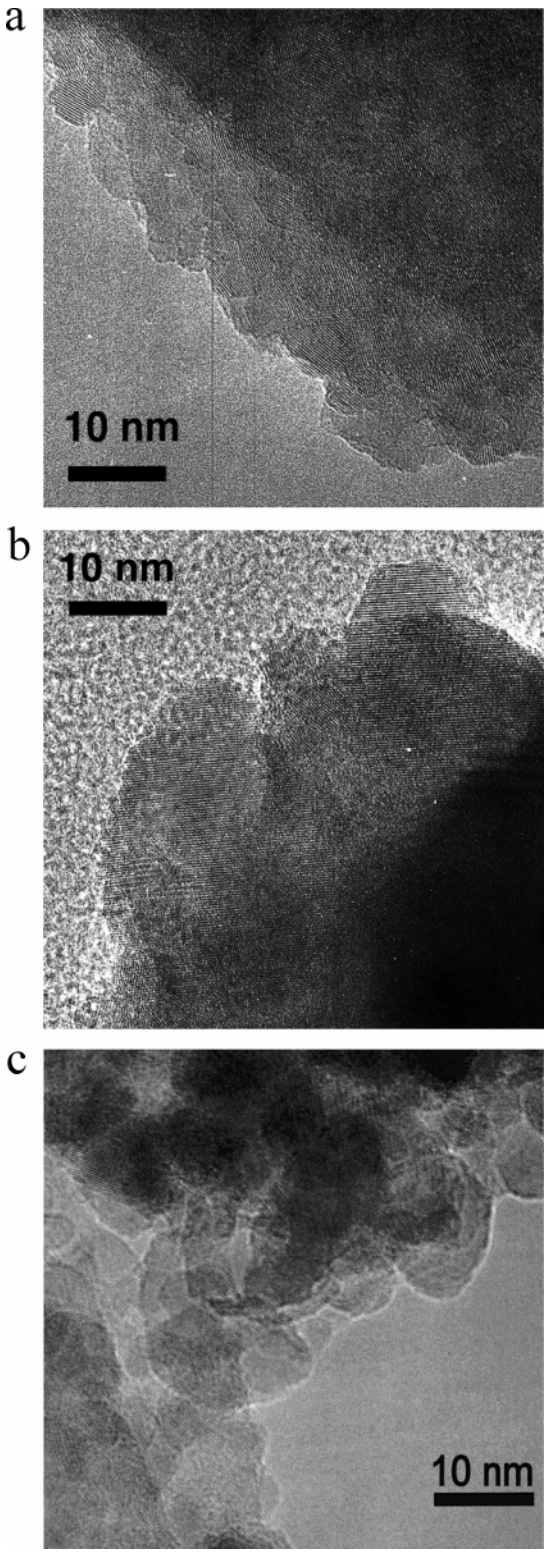

Figure 1. HRTEM images of ball-milled materials: (a) BM_{SA}, (b) BM_{SA+CO_2}, and (c) BM_{CO_2}.

and the nature of amorphous phases present in these materials as well as the extent of Cu/Zn interaction remains unclear. To complete the XRD and HRTEM results, X-ray absorption spectroscopy was performed.

3.2. XANES. *3.2.1. Cu K-edge.* Figure 3 shows that the background subtracted and normalized XANES spectra of the three ball-milled materials are all very different in terms of edge position, white line intensity, and shape of the resonance peaks

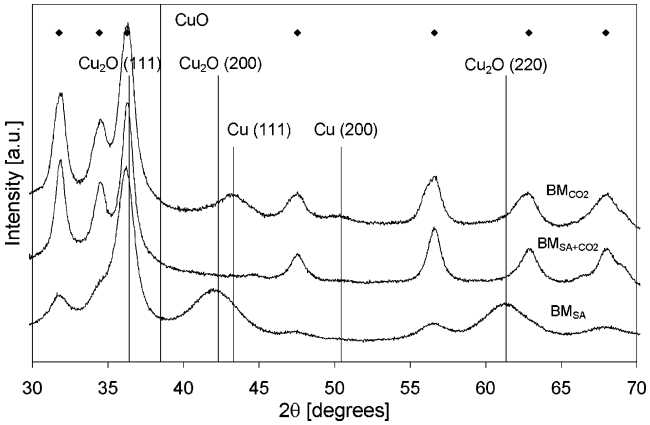

Figure 2. XRD patterns of ball-milled materials; ZnO peaks are represented by diamonds.

TABLE 1: Analytical Data of Cu_2O/ZnO Materials Ball Milled in Different Atmospheres[a]

material	% CuO TPR	% CuO EXAFS	% CO_3 TGA
BM_{SA}	98	100	
BM_{SA+CO_2}	94	80	33.4
BM_{CO_2}	34	48	31.4

[a] Reducible Cu determined by TPR[16] and EXAFS are expressed as % CuO. Carbonate is expressed as percentage O^{2-} transformed into CO_3^{2-} and includes the ZnO fraction.[16]

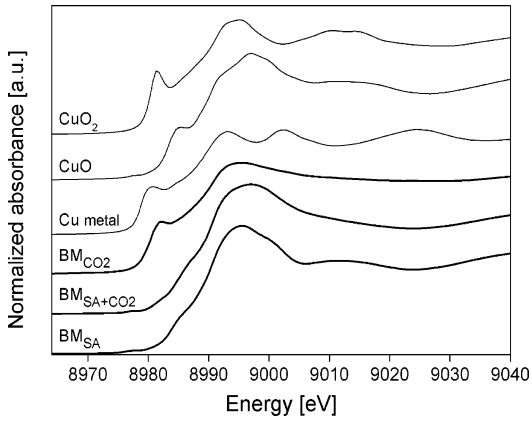

Figure 3. Cu K-edge background subtracted and normalized XANES spectra of ball-milled materials BM_{SA}, BM_{SA+CO_2}, BM_{CO_2}, and bulk reference samples Cu metal, CuO, and Cu_2O.

after the edge. In both BM_{SA} and BM_{SA+CO_2}, the edge position corresponding to the maximum of the first derivative (see below) is located at 8990.9 eV, which is typical of Cu^{2+} in bulk CuO. However, in the preedge region, the spectrum of BM_{SA+CO_2} is shifted toward somewhat lower energies suggesting the presence of some reduced copper species. The white line of BM_{SA+CO_2} is much broader than that of BM_{SA}, suggesting the presence of different phase compositions in these two catalysts. Among the three ball-milled materials, the profile of BM_{CO_2} is distinctly different from the other two. The white line intensity is significantly reduced and the edge position largely shifted toward a lower energy (8979.9 eV), whereas the resonance peaks after the edge are largely damped. The edge position clearly indicates that copper in BM_{CO_2} features a lower oxidation state than the Cu^{2+} state found in BM_{SA} and BM_{CO_2+SA}. Comparison of the preedge region shows that the BM_{CO_2} spectrum is positioned between the Cu foil and Cu_2O reference spectra, indicating the

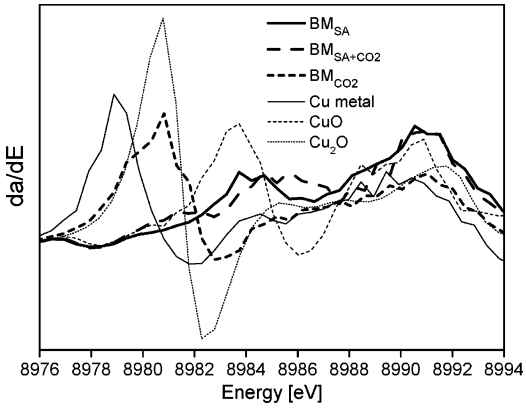

Figure 4. First derivative of the Cu K-edge background subtracted and normalized XANES spectra of ball-milled materials BM_{SA}, BM_{SA+CO_2}, BM_{CO_2}, and bulk reference samples Cu metal, CuO, and Cu_2O.

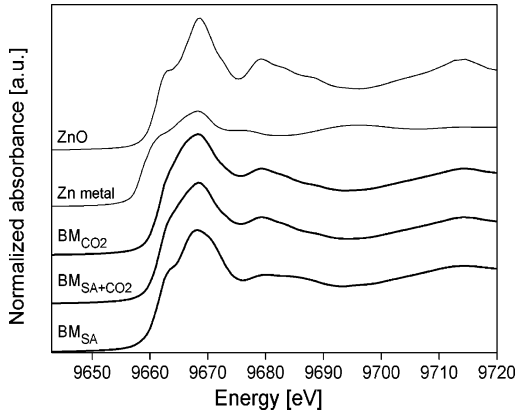

Figure 5. Zn K-edge background subtracted and normalized XANES spectra of ball-milled materials BM_{SA}, BM_{SA+CO_2}, BM_{CO_2}, and bulk reference samples Zn metal and ZnO.

presence of Cu^{1+} and/or Cu^0. The absence of the typical intense white line present in the oxides also strongly points toward the presence of metallic Cu in this material.

This preliminary analysis of the general shape of the XANES spectra shows that these materials are complex and contain different phases corresponding to different structures and/or copper oxidation states. Further details may be appreciated from the derivative of the XANES spectrum presented in Figure 4. The derivative of BM_{SA} is very similar to the one of the CuO reference compound, so the Cu phase of this material appears to be mainly composed of Cu^{2+}. In BM_{SA+CO_2}, the small bump located at 8980.3 eV and the shift toward higher energies of the shoulder at 8984.6 eV correspond to strong features in the Cu_2O reference sample. Clearly, a substantial amount of Cu^{1+} is present in the sample when milling takes place at a somewhat lower O_2 partial pressure with the addition of CO_2. This is in line with the lower TPR oxidation level found in this material compared with BM_{SA} (Table 1). Finally, BM_{CO_2} shows a remarkable profile with the main peak located at lower energies. As anticipated from the XANES profile, this peak obviously is a combination of the main features of the Cu metal and Cu_2O references. At the same time, the peak corresponding to Cu^{2+} at 8990.9 eV has lost intensity but has not disappeared completely, proving that, next to the Cu^0 and Cu^{1+} main phases in BM_{CO_2}, a small amount of a Cu^{2+} phase is present. Compared with the derivative of the CuO bulk reference, the shift toward higher energies of the peak at ca. 8984 eV found for the ball-milled materials is likely due to amorphization of the copper phase.

3.2.2. Zn K-edge. Figure 5 presents the background-subtracted and normalized XANES spectra at the Zn K-edge of the ball-milled materials. As expected, they feature roughly the same edge position that corresponds to Zn^{2+}. The spectra of BM_{SA+CO_2} and BM_{CO_2} are overlapping almost totally, showing that in these materials the Zn phase has exactly the same structure. Both spectra follow the oscillation of the ZnO reference compound with a slight damping, indicating that the materials still possess the basic structure of ZnO, but with a more nanosized and/or amorphous character. On the other hand, BM_{SA} features a distinctive profile indicating that part of the ZnO structure has undergone a significant transformation. In the derivatives (Figure 6), all samples feature a main peak located basically at the same energy of 9662 eV, that is, slightly higher than the main ZnO reference peak at 9661.5 eV. The second ZnO peak at 9665.9 eV is also present in BM_{SA} but very much damped in BM_{CO_2} and BM_{SA+CO_2}. Both the damping and the energy shift may be related to amorphization of the Zn phase by carbonate formation and ball milling.

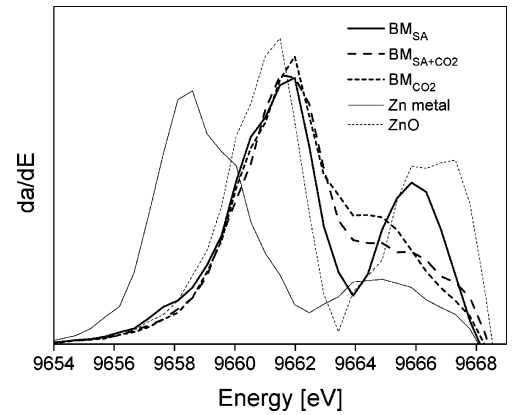

Figure 6. First derivative of the Zn K-edge background subtracted and normalized XANES spectra of ball-milled materials BM_{SA}, BM_{SA+CO_2}, BM_{CO_2}, and bulk reference samples Zn metal and ZnO.

3.3. EXAFS. The results of the EXAFS structural refinements are summarized in Tables 2 and 3 for the Cu and Zn K-edge measurements, respectively. The EXAFS best fits with *R* factors in the range of 12 to 30% for Cu and Zn K-edges are presented in Figures 7 and 8, while the corresponding Fourier transform (FT) best fits are presented in Figures 9 and 10.

3.3.1. Cu K-edge. The phase-corrected FTs of the EXAFS of the three samples at the Cu K-edge are given in Figure 11 along with the Cu, Cu_2O, and CuO reference samples. If they all present a first neighbor peak corresponding to an oxygen shell located at a distance of ca. 1.9 Å as in copper oxides, the exact position of this first coordination shell varies, with the shortest Cu−O distance found in BM_{CO_2}. The second coordination shell corresponding to Cu shells differs even more radically from one material to the other. In agreement with the XANES analysis, the most distinct material is BM_{CO_2} that presents a very intense second peak at ca. 2.5 Å, very close to the typical Cu−Cu distance in the copper metallic phase. The two other materials present a second peak at ca. 3.0 Å that corresponds roughly to the Cu coordination shell in both copper oxides. The intensity of this shell diminishes for increasing CO_2 partial pressure, suggesting that amorphization or transformation of the Cu phase into a more nanocrystalline material is related to the amount of CO_2 present during milling.

TABLE 2: Cu K-edge EXAFS Refinements of the Ball-milled Materials BM_{SA}, BM_{SA+CO_2}, and BM_{CO_2}, Including Bulk Copper Metal, Cuprite Cu_2O, and Tenorite CuO References

	bulk Cu	bulk Cu_2O	bulk CuO	BM_{SA}	BM_{SA+CO_2}	BM_{CO_2}
E_f (eV)[a]	−11.6 (9)	−9.5 (3)	1.1 (9)	4.1 (9)	6.0 (7)	−7.9 (8)
N_1[b]	12 Cu[f]	2 O[f]	4 O[f]	3.8 (3) O	3.5 (2) O	2.0 (1) O
R_1[c]	2.560 (2)	1.846 (3)	1.953 (7)	1.955 (7)	1.926 (5)	1.907 (6)
A_1[d]	0.017 (1)	0.007 (1)	0.014 (2)	0.017 (2)	0.015 (1)	0.016(2)
N_2	6 Cu[f]	12 Cu[f]	2 Cu[f]	6.6 (9) Zn	1.0 (3) Cu	1.8 (2) Cu
R_2	3.620 (3)	3.014 (5)	2.745 (9)	2.94 (1)	2.83 (2)	2.552 (4)
A_2	0.029 (6)	0.014 (3)	0.022 (8)	0.040 (6)	0.03 (2)	0.009 (2)
N_3	24 Cu[f]		4 Cu[f]		1.2 (3) Cu	0.7 (3) Cu
R_3	4.43 (1)		2.89 (3)		3.79 (3)	3.02 (1)
A_3	0.025 (2)		0.012 (8)		0.03 (2)	0.016 (9)
N_4	12 Cu[f]		4 Cu[f]			2.4 (6) Cu
R_4	5.12 (3)		3.08 (3)			3.63 (1)
A_4	0.023 (2)		0.019 (9)			0.032 (1)
N_5			2 Cu[f]			3.6 Cu (6)
R_5			3.43 (3)			4.46 (1)
A_5			0.02 (1)			0.023 (6)
N_6						3.0 (6) Cu
R_6						5.34 (1)
A_6						0.017 (7)
R (%)[e]	21.8	12.4	29.6	23.8	16.9	14.6

[a] E_f = contribution of the wave vector of the zero photoelectron relative to the origin of k (eV). [b] N_i = number of atoms in the ith shell. [c] R_i = radial distance of atoms in the ith shell (Å). [d] A_i = Debye−Waller term of the ith shell ($A = 2\sigma^2$ with σ = Debye−Waller Factor) (Å^2). [e] R factor in percent. [f] These parameters were kept fixed during the refinement. Bulk Cu: $Fm3-m$; $a = b = c = 3.615$ Å; 12 Cu at 2.556 Å, 6 Cu at 3.615 Å, 24 Cu at 4.427 Å, 12 Cu at 5.112 Å.[28] Bulk Cu_2O: $Pn3-mZ$ cuprite; $a = b = c = 4.267$ Å; 2 O at 1.848 Å, 12 Cu at 3.017 Å, 6 O at 3.538 Å, 6 Cu at 4.267 Å.[28] Bulk CuO: C12/C1 tenorite; $a = 4.6837$, Å $b = 3.4226$ Å, $c = 5.1288$ Å; 2 O at 1.951 Å, 2 O at 1.961 Å, 2 O at 2.784 Å, 4 Cu at 2.900 Å, 4 Cu at 3.083 Å, 2 Cu at 3.173 Å, 4 Cu at 3.423 Å, 2 Cu at 3.748 Å.[28]

TABLE 3: Zn K-edge EXAFS Refinements of the Ball-milled Materials BM_{SA}, BM_{SA+CO_2}, and BM_{CO_2}, Including Bulk Zincite ZnO

	bulk ZnO	BM_{SA}	BM_{SA+CO_2}	BM_{CO_2}
E_f (eV)[a]	−4.3(7)	1.1 (8)	−3.2 (9)	−1.1 (8)
N_1[b]	4 O[f]	4.4 (4) O	3.7 (4) O	3.6 (4) O
R_1[c]	1.968 (4)	1.980 (8)	1.964 (7)	1.962 (8)
A_1[d]	0.012 (2)	0.022 (3)	0.015 (2)	0.015 (3)
N_2	12 Zn[f]	2.4 (4) Cu	1.2 (3) C	1.4 (3) C
R_2	3.215 (6)	2.97 (2)	3.06 (9)	3.06 (8)
A_2	0.019 (1)	0.02 (4)	0.002 (9)	0.001 (9)
N_3	8 O[f]	3.4 (5) Zn	5.0 (8) O	4.0 (8) O
R_3	3.73 (2)	3.16 (3)	3.69 (5)	3.67 (3)
A_3	0.016 (6)	0.02 (3)	0.02 (1)	0.02 (1)
N_4	6 Zn[f]	4.6 (6) Zn	4.1 (6) Zn	4.6 (7) Zn
R_4	4.60 (2)	4.54 (8)	3.21 (2)	3.20 (2)
A_4	0.012 (4)	0.04 (2)	0.015 (2)	0.013 (3)
N_5		3.6 (6) O	4.7 (8) Zn	3.8 (8) Zn
R_5		3.56 (6)	4.54 (2)	4.53 (2)
A_5		0.03 (3)	0.02 (1)	0.02 (1)
N_6		4.0 (5) O		
R_6		4.25(6)		
A_6		0.002 (2)		
R (%)[e]	26.1	27.1	25.9	22.8

[a] E_f = contribution of the wave vector of the zero photoelectron relative to the origin of k (eV). [b] N_i = number of atoms in the ith shell. [c] R_i = radial distance of atoms in the ith shell (Å). [d] A_i = Debye−Waller term of the ith shell ($A = 2\sigma^2$ with σ = Debye−Waller Factor) (Å^2). [e] R factor in percent. [f] These parameters were kept fixed during the refinement. Bulk ZnO: zincite $P63mc$; $a = b = 3.2417$ Å, $c = 5.1876$ Å, 3 O at 1.969 Å, 1 O at 1.981 Å, 6 Zn at 3.188 Å, 1 O at 3.206 Å, 6 Zn at 3.242 Å, 8 O at 3.796 Å, 6 Zn at 4.554 Å.[28]

As anticipated, the fit of the first peak shows that Cu atoms in BM_{SA} and BM_{SA+CO_2} feature the same coordination of 3.6 O, while in BM_{CO_2} it has a low oxygen coordination number of 2.0. The bond distance, which varies from 1.955 Å in BM_{SA} to 1.910 Å in BM_{CO_2}, shows a constant decrease when the amount of SA in the mill vial is reduced. These distances correspond either roughly to the Cu−O bond distance in tenorite (1.951 Å) or to an average distance in a mixture of tenorite and cuprite phases that features a shorter Cu−O bond distance (1.848 Å).[28] Due to the strong Jahn−Teller effect that affects Cu^{2+} (d^9 configuration), the copper coordination in the CuO tenorite structure actually consists of highly elongated octahedra with two extra oxygens located at a distance of 2.78 Å. Since the contribution of the latter O shell is very weak—due to the long distance, low coordination, and high disorder—it was not considered in the EXAFS analysis.

The second peak in the FT could be fitted with 6.6 Cu or Zn atoms located at 2.94 Å from the Cu scatterer atom in BM_{SA} and two shells of ca. 1 Cu atom located at 2.83 and 3.79 Å in BM_{SA+CO_2}. Distinction between Cu and Zn is not possible due to their close scattering properties, phases, and amplitudes. In the latter material, these distances correspond to the averaged typical Cu−Cu bond distances in tenorite CuO (2.90 and 3.74 Å).[28] In BM_{SA}, the Cu−Cu bond distance of 2.94 Å also seems related to the Cu−Cu distance in tenorite CuO (2.90 Å).[28] However, the slight increase suggests some expansion of the lattice. The large coordination number of 6.6 Zn found in BM_{SA} compared to 1 Cu atom in BM_{SA+CO_2} clearly indicates a higher degree of crystallinity for the sample milled in pure SA. This coordination number is bigger than the value of 4 expected in the tenorite phase, even when one takes into account the large deviation associated with this shell. The high Debye−Waller factor indicates a significant disorder around the copper atoms. The large coordination numbers and bond distance corresponding to this second shell in BM_{SA} suggest the formation of an oxidic phase different from the CuO or Cu_2O phase in this material.

BM_{CO_2} presents a totally different structure than the other materials with a shell of 1.8 Cu at 2.55 Å. This shell does not belong to any copper oxide structure but corresponds roughly to the typical Cu−Cu distance of the metallic phase (2.56 Å).[28] This is in good agreement with the diffraction measurements that have already pointed out the presence of a Cu metallic phase

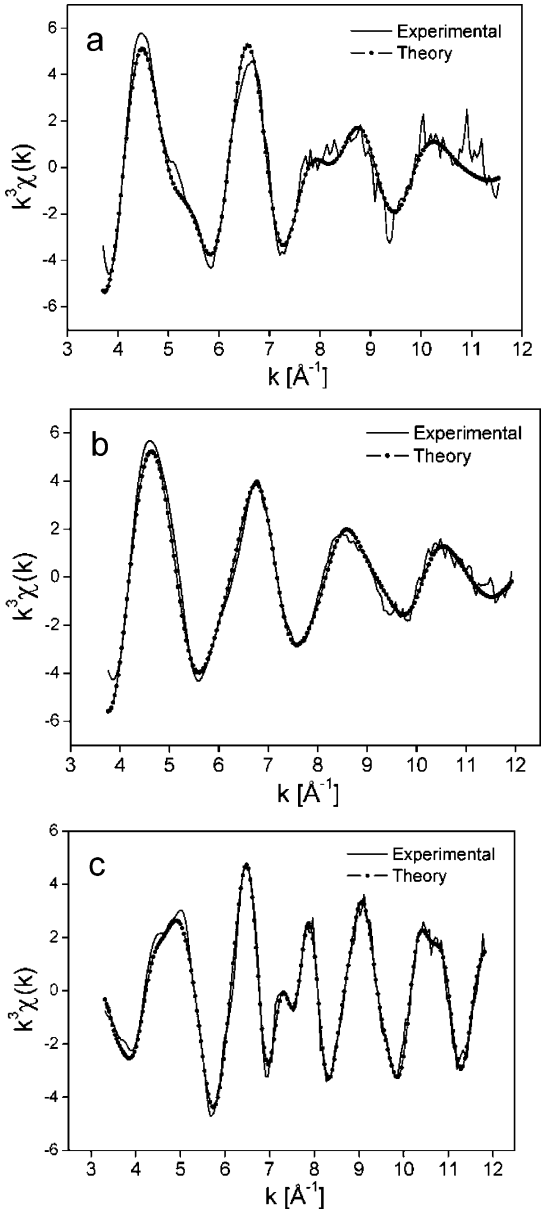

Figure 7. Cu K-edge EXAFS spectra (after background subtraction, k^3-weighted) of ball-milled materials: (a) BM_{SA}, (b) BM_{SA+CO_2}, and (c) BM_{CO_2}. Solid lines are the experimental data, and dotted lines are the best fit.

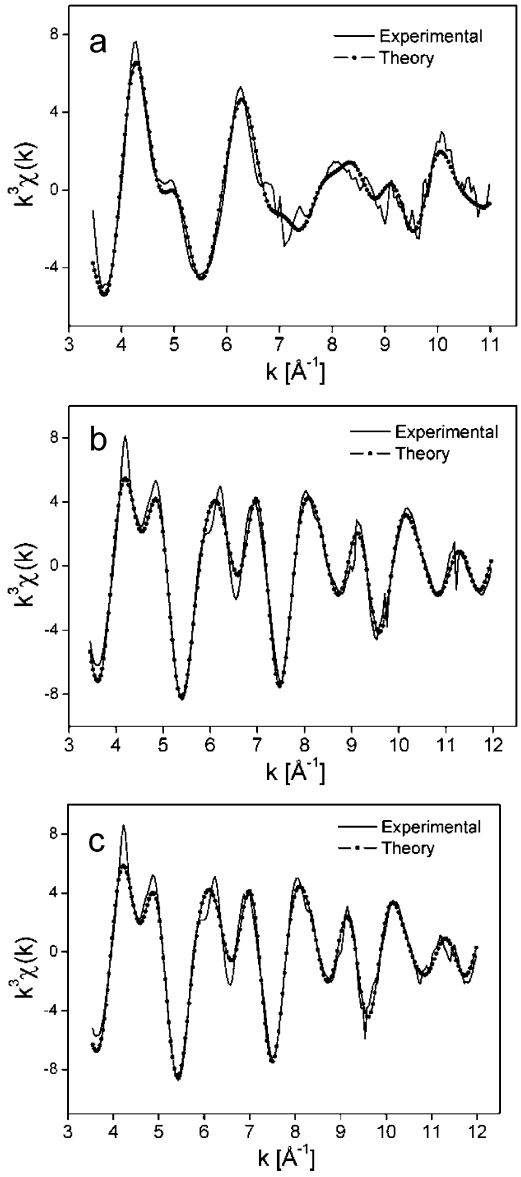

Figure 8. Zn K-edge EXAFS spectra (after background subtraction, k^3-weighted) of ball-milled materials: (a) BM_{SA}, (b) BM_{SA+CO_2}, and (c) BM_{CO_2}. Solid lines are the experimental data, and dotted lines are the best fit.

in this material. The total coordination of the first shells in this material is unusually low with 2.0 O and 1.8 Cu. To correct for the anharmonic motion of surface atoms in small Cu particles,[29] a cumulant expansion was introduced in the fitting. The remaining shell in BM_{CO_2} could be fitted with 0.7 Cu at 3.02 Å, corresponding to the typical Cu−Cu bond distance in cuprite Cu_2O (3.02 Å).[28] In addition, the fit shows the presence of peaks at higher R values (3.63, 4.46 and 5.34 Å) corresponding to the typical Cu−Cu bond distances in the copper metal structure.

As by means of the EXAFS technique, bond distances can be determined with high accuracy (±0.02 Å), the Cu−O distance can be used to evaluate the extent of oxidation as well as the relative amount of the different phases.[30,31] If we consider that copper is mainly coordinated to 4 O located at 1.95 Å in bulk tenorite CuO and to 2 O at 1.85 Å in cuprite Cu_2O, the fractions δ_{CuO} and δ_{Cu2O} of the two phases in the ball-milled materials can be estimated using the Cu−O bond distance R_{Cu-O} determined with EXAFS, weighted by their coordination number. Solving the equations

$$R_{Cu-O} = (4 \times 1.95 \times \delta_{CuO} + 2 \times 1.85 \times \delta_{Cu2O})/(4 \times \delta_{CuO} + 2 \times \delta_{Cu2O})$$

and

$$\delta_{CuO} + \delta_{Cu2O} = 1$$

gives the respective Cu^{2+} fractions of the total Cu oxide phase of 100% in BM_{SA}, 61% in BM_{SA+CO_2}, and 40% in BM_{CO_2}. In BM_{SA+CO_2} that is only composed of copper oxide phases, the remaining phase is simply 39% of Cu_2O. The corresponding degrees of Cu reduction are presented in Table 1 along with the values derived from the TPR measurements. The results obtained from both techniques are in good agreement, although the values of BM_{CO_2} show a larger discrepancy. Although coordination numbers in EXAFS are generally determined with

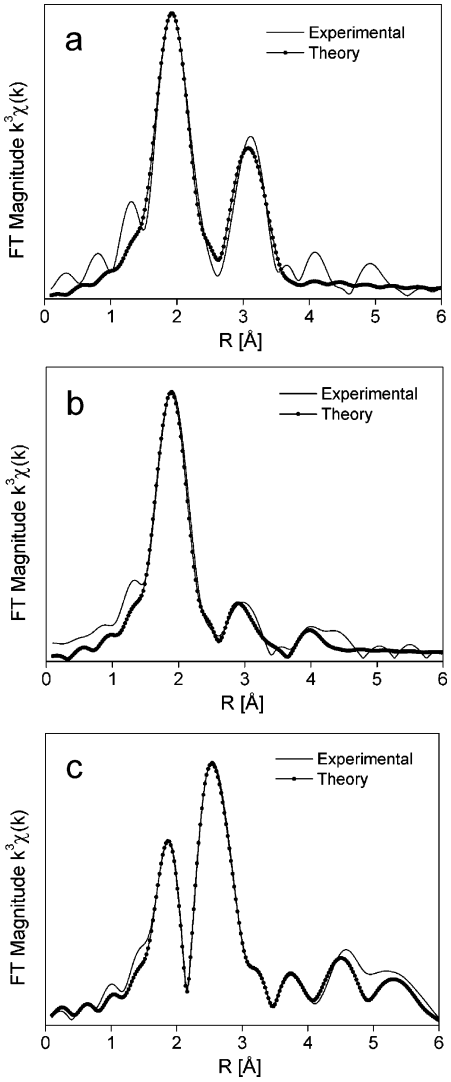

Figure 9. Fourier transforms of the Cu K-edge k^3-weighted EXAFS of ball-milled materials: (a) BM_{SA}, (b) BM_{SA+CO_2}, and (c) BM_{CO_2}. Solid lines are the experimental data, and dotted lines are the best fit.

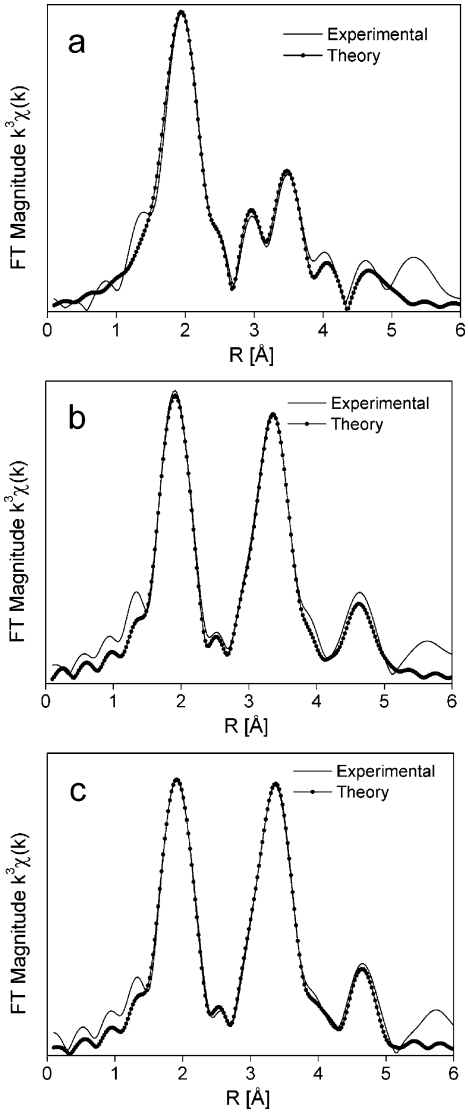

Figure 10. Fourier transforms of the Zn K-edge k^3-weighted EXAFS of ball-milled materials: (a) BM_{SA}, (b) BM_{SA+CO_2}, and (c) BM_{CO_2}. Solid lines are the experimental data, and dotted lines are the best fit.

much less accuracy (±20%) than the distances, the amount of copper metal in BM_{CO_2} can be estimated by comparing the total oxygen coordination number

$$N_{oxy} = 4 \times \delta_{CuO} + 2 \times \delta_{Cu2O} = 2.9$$

and the coordination number of 2.0 found by fitting. This gives a fraction of 2/2.9 ≈ 69% of the Cu atoms belonging to the oxidic phases and 31% to the metallic phase. The fractions of the Cu^0, Cu^{1+}, and Cu^{2+} phases in BM_{CO_2} are then ca. 31, 41, and 28%, respectively.

3.3.2. Zn K-edge. The phase-corrected FTs corresponding to the EXAFS measurements at the Zn K-edge of the three ball-milled materials are presented in Figure 12 along with the ZnO reference sample. In accordance with the XANES analysis, the BM_{CO_2} and BM_{SA+CO_2} materials are very similar with almost overlapping FTs. In BM_{SA}, the FT profile exhibits a distinct shape with very low intensity in the high-*R* region, indicating a more disordered Zn phase. Interestingly, this sample exhibited the most ordered Cu phase. The FT profiles of BM_{CO_2} and BM_{SA+CO_2} match that of the ZnO reference compound with three main peaks located at ca. 1.9, 3.4, and 4.7 Å, corresponding to an O shell and two multi-peaks with Zn and O contributions. The low intensity of the second and third peak indicates amorphization and/or formation of nanosize crystallites, as can be expected after ball milling.

These preliminary observations are confirmed by the EXAFS refinements presented in Table 3. In BM_{SA+CO_2} and BM_{CO_2}, the first peak could be fitted with ca. 3.6 O located at 1.96 Å, corresponding to the 4-fold O coordination and Zn−O bond distance in bulk ZnO. The peaks in the FT of these two materials at distances of ca. 3.2 and 4.5 Å correspond to the typical Zn−Zn bond distances in bulk ZnO of 3.215 and 4.594 Å. However, the coordination numbers associated with these shells of 4−5 are significantly smaller than the expected values of 12 and 6 in the bulk structure, again pointing out the amorphous and/or nanocrystalline character of these materials.

In both materials ball milled with CO_2, the fit was greatly improved by adding a carbon coordination shell of 1.2−1.4 atoms located at 3.06 Å. This distance corresponds roughly to the first Zn−C bond distance in the smithsonite structure of zinc carbonate $ZnCO_3$ (2.964 Å)[28] and even more accurately to that in the hydrozincite structure $Zn_5(OH)_6CO_3$ (3.07 Å).[28] This latter option is less realistic in view of the TGA-MS results that did not reveal any water desorption. However, the first

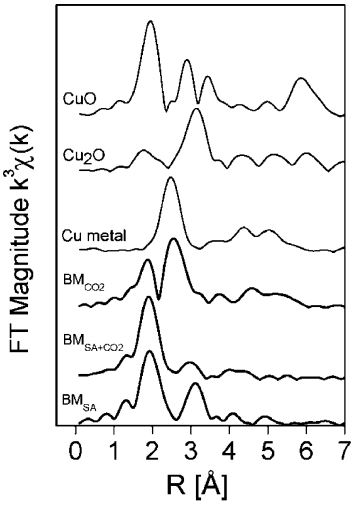

Figure 11. Fourier transforms of the Cu K-edge k^3-weighted EXAFS of ball-milled materials and bulk reference samples.

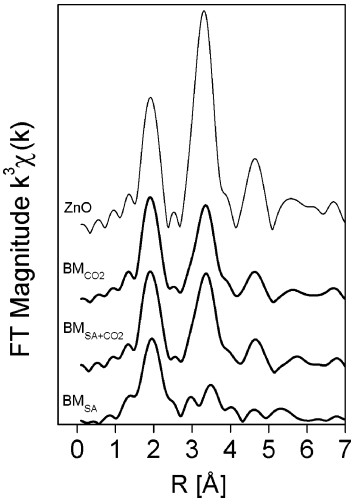

Figure 12. Fourier transforms of the Zn K-edge k^3-weighted EXAFS of ball-milled materials and bulk reference ZnO.

coordination shell Zn−O bond distances of 2.11 Å in smithsonite and 2.06 Å in hydrozincite are much longer than the distance of 1.96 Å found in the refinement of BM_{CO_2} and BM_{SA+CO_2}. Thus, the formation of one of these phases during ball milling can be excluded. A plausible explanation for the existence of an extra C shell could be the formation of a superficial amorphous mixed Zn-oxide/carbonate layer. Considering the large quantities of carbonate involved (Table 1), one could envisage this layer to be primarily located in the grain boundaries that generally exhibit a strongly disordered structure. This explanation would be in line with the TGA-MS results and the XRD patterns that exhibit a strong amorphous background.

In BM_{SA}, the average oxygen coordination number has increased to 4.4 whereas the Zn−O bond distance of 1.98 Å is significantly longer than those found in BM_{SA+CO_2} and BM_{CO_2}. The high coordination number suggests that this material may consist of a mixture of ZnO with 4-fold coordination and another phase in which Zn has a 6-fold coordination. This assumption is confirmed by the presence of a second peak that could be fitted with a shell of 2.4 Zn/Cu atoms at a distance of 2.97 Å, which does not correspond to the first Zn−Zn bond distances (3.19 and 3.24 Å) in the bulk ZnO either. The second and the third Zn−Zn peaks at 3.16 and 4.54 Å are more closely related to the typical Zn−Zn distances in bulk ZnO (3.19, 3.24, and 4.55 Å). All Zn−Zn bond distances are slightly shorter than the corresponding bulk values, indicative of a strongly defective ZnO structure in this ball-milled material. The low coordination numbers associated with the second and third shell clearly indicate that the Zn phase in this material features the most amorphous structure of the three ball-milled materials. Additionally, these results point toward the transformation of a significant part of the ZnO phase into another phase, as the XRD analysis already suggested.

3.4. Overview of the Structures Formed by Ball Milling. Comparison of the results obtained at the Cu and Zn K-edges of the BM_{SA} material reveals that the second metal−metal shells are located at a very similar bond distance of 2.94 Å around Cu atoms and 2.97 Å around Zn atoms. This distance lies between the first Cu−Cu distances in tenorite CuO (2.90 Å) and in cuprite Cu_2O (3.017 Å) and is much shorter than the Zn−Zn distance in ZnO (3.20 Å). Moreover, at both edges, the metal−O bond distances are slightly longer than the expected values for CuO or ZnO phases, indicating that another phase is likely formed during ball milling. The elongation is smaller for Cu, which might indicate the presence of a slightly different environment around the Cu and Zn atoms in this phase. A second explanation would be the additional presence of a CuO-type phase, which features shorter Cu−O and Cu−Cu bond distances.

A plausible interpretation of these elements combined with the XRD data is the formation of a nanocrystalline/amorphous $Cu_{1-x}Zn_xO$ type solid solution based on the incorporation of Zn^{2+} in the Cu oxide matrix during ball milling in SA. Several types of crystalline solid solutions formed during the preparation of Cu/ZnO catalysts have already been reported in the literature: Cu^{2+}/ZnO, Cu^{1+}/ZnO, and Zn^{2+}/CuO.[32−37] Although temperatures as different as 350 °C[37] and 1000 °C[34−36] have been reported for the formation of the last solid solution, all authors agree upon a very low solubility limit of 3−5 mol % Zn^{2+} in the tenorite structure.

Contrarily, the miscibility of Zn in NiO can reach 40% when heated to temperatures >1000 °C,[38] which is explained by defect formation in the NiO and ZnO lattices. NiO takes up excess oxygen during heating in air, which leads to the migration of Ni ions to the surface and the creation of cation vacancies. At the same time, ZnO loses oxygen at the surface by dissociation, leaving excess Zn^0 behind which diffuses into interstitial lattice positions. This process results in growth of the cubic (Ni, Zn)O phase and a simultaneous disappearance of the ZnO phase. As the reaction proceeds, the lattice parameter increases due to the larger size of Zn^{2+}, namely, 60 pm as compared with 55 pm for Ni^{2+}. Despite the similar size of 57 pm for Cu^{2+}, previous work[32−37] has shown that CuO does not form highly mixed solid solutions with ZnO. This may be explained by the different crystalline systems: rock salt for NiO and monoclinic for CuO. The latter structure is explained by the occurrence of a strong Jahn−Teller effect in Cu^{2+} that is considerably distorting the Cu octahedral geometry.

As Cu_2O is prone to form nonstoichiometric phases[39] and behaves similarly to NiO when heated,[38] it should in principle be able to incorporate large amounts of Zn^{2+} in its structure. The first metal−metal bond distance of 2.98 Å in $Ni_{0.6}Zn_{0.4}O$ is larger than the Ni−Ni bond distance of 2.956 Å[28] in NiO. Interestingly, this size is similar to the metal−metal distances found in BM_{SA} at the Cu (2.94 Å) and Zn K-edge (2.97 Å). The slightly shorter distance at the Cu K-edge might be explained by the presence of a CuO phase with a Cu−Cu bond

TABLE 4: Phase Compositions of Ball-milled Materials BM_{SA}, BM_{SA+CO_2}, and BM_{CO_2}

material	Cu^0	Cu^{1+}	Cu^{2+}	Zn^{2+}
BM_{SA}			$CuO/Cu_{1-x}Zn_xO$ ($x \approx 0.3$; distorted rock salt)	$ZnO/Cu_{1-x}Zn_xO$ ($x \approx 0.3$; distorted rock salt)
BM_{SA+CO_2}		40% Cu_2O	60% CuO/Cu−carbonate[16]	100% ZnO/Zn−carbonate
BM_{CO_2}	31% Cu metal	41% Cu_2O	28% CuO/Cu−carbonate[16]	100% ZnO/Zn−carbonate

distance of 2.90 Å that cannot be separated out in the fitting process. The coordination number of 6.6 at the Cu K-edge is much bigger than the typical coordination of 4 in bulk CuO and also in favor of a solid solution. Finally, the relatively large metal coordination number of 2.4 found at the Zn K-edge means that the amount of Zn^{2+} in this solid solution is much higher than the maximum of 5 mol % found in the CuO tenorite matrix.

The XAS data can be brought in accordance with the XRD pattern by assuming that a Cu^{2+}-based $Cu_{1-x}Zn_xO$ solid solution is formed that retains almost the same metallic face centered cubic (fcc) lattice as Cu_2O. Indeed, simulation of the cuprite diffraction pattern, which can be described as an fcc lattice of Cu ions penetrating a body centered cubic (bcc) oxygen lattice, showed that the main (111), (200), and (220) reflections at $2\Theta = 36$, 42, and 61° are mainly due to the scattering of the fcc Cu atoms. Removal of the oxygen lattice causes minor changes in these reflections intensities. This means that this solid solution may be formed by incorporation of Zn^{2+} and O^{2-} in the Cu_2O structure and the concomitant oxidation of Cu^{1+} into Cu^{2+}. In this respect, the $Cu_{1-x}Zn_xO$ solid solution is similar to the rock salt $Ni_{1-x}Zn_xO$ solid solution. However, this structure is significantly distorted, since Zn and Cu feature different octahedral geometries as indicated by EXAFS and display substantial amorphicity as indicated by the width of the diffraction peaks. The transformation of part of the Zn atoms from the 4-fold coordinated ZnO phase into the 6-fold coordination of the fcc phase is clearly seen in EXAFS by the increase of the average coordination from 3.8 in ZnO to 4.4 in BM_{SA} and the elongation of the Zn−O distance from 1.96 to 1.98 Å. The Cu atom coordination also increases markedly from 2 in Cu_2O to a highly distorted 6-fold coordination in the fcc phase with 3.6 O located at 1.96 Å as in bulk CuO and 2 O at 2.8 Å not included in the EXAFS fit (see above). Evaluation of the Zn content in $Cu_{1-x}Zn_xO$ can be achieved from the average Zn−O coordination of 4.4. The metal fraction would correspond to a mixture of 80% Zn in 4-fold coordination and 20% in 6-fold coordination. Considering the initial Cu/Zn ratio of 30/70, this means that based on total metal $0.7 \times 20 = 14\%$ is forming a solid solution with Cu. Assuming all Cu atoms to be incorporated into this phase, the Zn fraction in the solid solution amounts to $14/(30 + 14) = 0.32$, that is, much larger than 3−5 mol % reported for CuO-based solid solutions. The intensity ratios 1.00, 0.80, and 0.86 of the main Cu (111), (200), and (220) reflections were obtained by fitting the XRD pattern with Gaussians and subtracting the ZnO (101) contribution. The fact that the ratio of these intensities differs from that in Cu_2O (1.00, 0.36, and 0.35) illustrates that the high disorder of this new phase significantly affects the relative intensities of the main reflections. Although the formation of a highly mixed solid solution similar to the one formed in the Ni/Zn system has never been achieved by mixing CuO and ZnO, the present results indicate that it is possible to form such a phase by ball milling Cu_2O and ZnO. The dissolution of ZnO might proceed more readily in the Cu fcc sublattice of Cu_2O, explaining why the formation of Cu/Zn oxide solid solutions with a high Zn content is not possible when starting from the monoclinic CuO phase.

An average view of the local structure around Cu and Zn atoms determined with EXAFS cannot give any direct information on the morphology of these particles. However, combined with the HRTEM and XRD results, it is possible to propose structural models for the three different materials. In BM_{CO_2}, ball milling induces the disproportionation of Cu_2O with ca. 31% of the copper-forming metallic particles. These particles are protected from oxidation by a Cu_2O-type oxide interface layer accounting for ca. 40% of the Cu atoms and a CuO-type shell accounting for ca. 28% of the Cu atoms. These oxidic phases may serve as an interface between the metallic Cu and ZnO phases. The Cu oxide phases are likely to consist of a (mixed) carbonate and are rather amorphous, as XRD showed no clear peaks corresponding to any of these structures. Finally, these aggregates are covered with a ZnO-type phase that may form a mixed amorphous carbonate interface at the surface of the CuO phase but largely remains nanocrystalline as observed from the XRD peaks and structure observed by HRTEM. EXAFS also showed that a large part of the Zn atoms forms a superficial amorphous mixed oxide/carbonate at the grain boundaries, accompanied by the disproportionation of Cu_2O. Remarkably, the extent of disproportionation found in Cu_2O/ZnO material ball milled under vacuum was much smaller,[16] indicating that this effect is related to the formation of this Zn amorphous carbonate phase. One explanation could be that the metal oxidation state is better preserved for carbonates, enhancing the reduction of the remaining oxidic part.

When the Cu_2O/ZnO starting mixture is ball milled under a mixed $SA + CO_2$ atmosphere, the same processes seem to occur, except that in this case O_2 seems to limit the disproportionation of Cu_2O into metallic copper. Instead, ca. 61% of the original Cu_2O material is oxidized to Cu^{2+}. The copper phase in this material was found to be almost entirely amorphous. Although some mixing of the Cu and Zn phases accompanied by carbonate formation may be expected in this material, no clear evidence was found in this XAS analysis.

In BM_{SA}, the Cu phase is almost completely oxidized to Cu^{2+} and the Cu/Zn interaction is much stronger. About half of the Cu and Zn appear to have formed a distorted solid solution that has never been reported before. Zn and O atoms are incorporated into the Cu_2O cuprite structure, while the Cu-oxidation state changes from Cu^{1+} to Cu^{2+}. In this solid solution, Zn and Cu feature an octahedral coordination with different geometries. The distorted fcc structure would be similar to the $Ni_{1-x}Zn_xO$ solid solution ($x \approx 0.5$), as indicated by the broad reflections in the XRD pattern that correspond roughly to the Cu fcc sublattice in Cu_2O. The morphology of this material probably consists of a succession of layers. Starting from an amorphous CuO-type core surrounded by a disordered rock salt $Cu_{1-x}Zn_xO$ solid solution of Zn in the Cu_2O matrix, an amorphous ZnO layer is found that is covered up by remaining ZnO nanocrystallites that have not reacted. A summary of the compositions of the ball-milled materials is given in Table 4.

Except in the ball-milled—mechanochemically prepared—materials investigated here, the transient existence of similar highly mixed structures can be expected during preparation, calcination, and activation of various types of Cu/ZnO catalysts.

Although the formation of large amounts of these highly mixed phases in thermochemically activated—that is, under reaction conditions—Cu/ZnO catalysts is not likely, small amounts may still be present depending on the oxidative power of the gas atmosphere. While high local temperatures can be reached for short periods during ball milling, high temperatures persist continuously for catalysts in their activated state and lead to a more rapid decay of the solid surface species. Moreover, due to their localized character and small quantities, detection of such surface species may be less straightforward than in the present case. In the Cu/ZnO system, activity is closely related both to the oxidation state of Cu[3,5] and to the presence of ZnO, which is often defective and may be involved in alloy formation.[4,6,7] Several models have been proposed to describe the relation between the two, for example, ZnO assisting Cu in keeping the desired oxidation state or Cu ensuring ZnO in being sufficiently defective. Consequently, the occurrence of mixed Cu/Zn oxide phases in the Cu/ZnO system is of great interest for the general understanding of the catalytic mechanism. Likewise, disproportionation reactions may readily occur in synthesis gas under reaction conditions and may thus play a role in the formation of mixed Cu/Zn metallic phases during the activation/reduction process. For these reasons, despite the differences in the activation processes, the structures found here should seriously be taken into account when considering both the bulk and the surface of these materials when exposed to reaction mixtures.

4. Conclusions

The combination of X-ray absorption techniques, HRTEM, and XRD is very powerful to investigate the multiphased amorphous and/or nanocrystalline structure of catalytic materials. This XAS study is a significant contribution to the understanding of the nature and relative amounts of the phases in mechanically milled Cu_2O/ZnO materials by a thorough characterization of their structure. The results showed that these materials have a more complex structure than was originally assumed using diffraction techniques.

Reduction of the crystallite size to the nanosize range and/or amorphization typical of mechanical milling is found for all materials, although different reactions are observed depending on the oxidative power of the milling atmosphere. Ball milling in pure CO_2 induces the disproportionation of Cu into Cu^0, Cu^{1+}, and Cu^{2+}. The additional presence of SA leads to a mixture of equal parts of Cu^{1+} and Cu^{2+}. An amorphous mixed oxide/carbonate phase is formed in these materials. Zn does not interact strongly with the copper phase, although mixing is enhanced at the grain boundaries due to the loose binding between the Cu and Zn species. We found strong indications that ball milling in SA induces oxidation of Cu into a distorted, nanocrystalline Cu^{2+}-based $Cu_{1-x}Zn_xO$ solid solution with a high miscibility of Zn in the Cu fcc sublattice of the Cu_2O structure.

Formation of a highly mixed Cu/Zn oxidic disordered solid solution was shown for the first time and indicates that the Cu/Zn interaction may be much stronger than generally assumed. It is speculated that this solid solution can also be present in the bulk or at the surface of activated Cu/ZnO catalysts prepared by conventional methods. Similarly, disproportionation reactions may be involved in the formation of mixed Cu/Zn metallic phases during the activation/reduction process. Consequently, the phases and solid−gas reactions observed in this study merit special attention in future spectroscopic work.

Acknowledgment. For financial support, we thank The Netherlands Organization for the Advancement of Research NWO (Project Nos. 047.015.004 and 047.005.03.96), the Dutch foundation for Fundamental Research on Matter, and the Utrecht University XAFS user support group. Access to the synchrotron facilities at the ESRF (BM26 DUBBLE-experiment 26-01-192) was arranged through the general support of NWO, and we wish to acknowledge the assistance and advice of Sergey Nikitenko during the measurements. The authors thank Patricia Kooijman of the National Centre for High Resolution Electron Microscopy at the Delft University of Technology for performing electron microscopy investigations. Erdny Batyrev, Jurriaan Beckers, and Vladimir Pelipenko are acknowledged for their assistance in the EXAFS measurements. We also wish to acknowledge the use of the EPSRCs Chemical Database Service at Daresbury.

References and Notes

(1) Poels, E.; Brands, D. *Appl. Catal., A* **2000**, *191*, 83.
(2) Brands, D. S.; Poels, E. K.; Krieger, T. A.; Makarova, O. V.; Weber, C.; Veer, S.; Bliek, A. *Catal. Lett.* **1995**, *36*, 175.
(3) Klier, K. *Adv. Catal.* **1982**, *31*, 243.
(4) Frost, J. C. *Nature* **1988**, *334*, 577.
(5) Chinchen, G. C.; Waugh, K. C.; Whan, D. A. *Appl. Catal.* **1986**, *25*, 101.
(6) Fujitani, T.; Nakamura, J. *Appl. Catal., A* **2000**, *191*, 111.
(7) Nakamura, J.; Choi, Y.; Fujitani, T. *Top. Catal.* **2003**, *22*, 277.
(8) Spencer, M. S. *Catal. Today* **1992**, *12*, 453.
(9) Waller, D.; Stirling, D.; Stone, F. S.; Spencer, M. S. *Faraday Discuss. Chem. Soc.* **1989**, *87*, 107.
(10) Fujita, S.; Satriyo, A. M.; Shen, G. C.; Takezawa, N. *Catal. Lett.* **1995**, *34*, 85.
(11) Mulas, G.; Varga, M.; Bertóti, I.; Molnár, A.; Cocco, G.; Szépvölgyi, J. *Mater. Sci. Eng., A* **1999**, *267*, 193.
(12) Lin, G. I.; Samokhin, P. V.; Kaloshkin, S. D.; Rozovskii, A. Y. *Kinet. Catal.* **1998**, *39*, 577.
(13) Brower, W. E.; Montes, A. J.; Prudlow, K. A.; Bakker, H.; Moleman, A. C.; Yang, H. *Mater. Sci. Forum* **1997**, *235*−*238*, 935.
(14) Takacs, L. *Prog. Mater. Sci.* **2002**, *47*, 355.
(15) Castricum, H. L.; Bakker, H.; Poels, E. K. *Mater. Sci. Eng., A* **2001**, *304*, 418.
(16) Castricum, H. L.; Bakker, H.; van der Linden, B.; Poels, E. K. *J. Phys. Chem. B* **2001**, *105*, 7928.
(17) Suryanarayana, C. *Prog. Mater. Sci.* **2001**, *46*, 1.
(18) Bakker, H.; Zhou, G. F.; Yang, H. *Prog. Mater. Sci.* **1995**, *39*, 159.
(19) Skarman, B.; Grandjean, D.; Benfield, R. E.; Hinz, A.; Andersson, A.; Wallenberg, L. R. *J. Catal.* **2002**, *211*, 119.
(20) Clausen, B. S. *Catal. Today* **1998**, *39*, 293.
(21) Clausen, B. S.; Grabaek, L.; Steffensen, G.; Hansen, P. L.; Topsoe, H. *Catal. Lett.* **1993**, *20*, 23.
(22) Clausen, B. S.; Topsoe, H. *Catal. Today* **1991**, *9*, 189.
(23) Grunwaldt, J. D.; Molenbroek, A. M.; Topsoe, N. Y.; Topsoe, H.; Clausen, B. S. *J. Catal.* **2000**, *194*, 452.
(24) Gunter, M. M.; Ressler, T.; Bems, B.; Buscher, C.; Genger, T.; Hinrichsen, O.; Muhler, M.; Schlogl, R. *Catal. Lett.* **2001**, *71*, 37.
(25) Meitzner, G.; Iglesia, E. *Catal. Today* **1999**, *53*, 433.
(26) Gunter, M. M.; Ressler, T.; Jentoft, R. E.; Bems, B. *J. Catal.* **2001**, *203*, 133.
(27) Binsted, N.; Campbell, J. W.; Gurman, S. J.; Stephenson, P. C. *EXAFS Analysis Programs*; Daresbury Laboratory: Warrington, U.K., 1991.
(28) Fletcher, D. A.; McMeeking, R. F.; Parkin, D. *J. Chem. Inf. Comput. Sci.* **1996**, *36*, 746.
(29) Clausen, B. S.; Norskov, J. K. *Top. Catal.* **2000**, *10*, 221.
(30) Barrett, P. A.; Sankar, G.; Catlow, C. R. A.; Thomas, J. M. *J. Phys. Chem.* **1996**, *100*, 8977.
(31) Grandjean, D.; Benfield, R. E.; Nayral, C.; Maisonnat, A.; Chaudret, B. *J. Phys. Chem. B* **2004**, *108*, 8876.
(32) Plyasova, L. M.; Yurieva, T. M. *Sib. Khim. Zh.* **1993**, *1*, 96.
(33) Bulko, J. B.; Herman, R. G.; Klier, K.; Simmons, G. W. *J. Phys. Chem.* **1979**, *83*, 3118.
(34) Delorme, C. *Bull. Chem. Franc. Miner. Crist.* **1958**, *81*, 19.
(35) Porta, P.; Derossi, S.; Ferraris, G.; Pompa, F. *Solid State Ionics* **1991**, *45*, 35.
(36) Cernak, J.; Gerard, F.; Kappenstein, C.; Chomic, J. *Monatsh. Chem.* **2004**, *135*, 1081.
(37) Ketchik, S.; Minyukova, T.; Kuznetsova, L.; Plyasova, L.; Yurieva, T.; Boreskov, G. *React. Kinet. Catal. Lett.* **1982**, *19*, 345.
(38) Kedesdy, H.; Drukalsky, A. *J. Am. Chem. Soc.* **1954**, *76*, 5941.
(39) Dunwald, H.; Wagner, C. *Z. Phys. Chem.* **1933**, *22B*, 212.